Biomacromolecules

pubs.acs.org/Biomac

Article

Electron Tomography and Machine Learning for Understanding the Highly Ordered Structure of Leafhopper Brochosomes

Gabriel R. Burks, Lehan Yao, Falon C. Kalutantirige, Kyle J. Gray, Elizabeth Bello, Shreyas Rajagopalan, Sarah B. Bialik, Jeffrey E. Barrick, Marianne Alleyne, Qian Chen, and Charles M. Schroeder*

Cite This: *Biomacromolecules* 2023, 24, 190−200

Read Online

ACCESS | Metrics & More | Article Recommendations | Supporting Information

ABSTRACT: Insects known as leafhoppers (Hemiptera: Cicadellidae) produce hierarchically structured nanoparticles known as brochosomes that are exuded and applied to the insect cuticle, thereby providing camouflage and anti-wetting properties to aid insect survival. Although the physical properties of brochosomes are thought to depend on the leafhopper species, the structure−function relationships governing brochosome behavior are not fully understood. Brochosomes have complex hierarchical structures and morphological heterogeneity across species, due to which a multimodal characterization approach is required to effectively elucidate their nanoscale structure and properties. In this work, we study the structural and mechanical properties of brochosomes using a combination of atomic force microscopy (AFM), electron microscopy (EM), electron tomography, and machine learning (ML)-based quantification of large and complex scanning electron microscopy (SEM) image data sets. This suite of techniques allows for the characterization of internal and external brochosome structures, and ML-based image analysis methods of large data sets reveal correlations in the structure across several leafhopper species. Our results show that brochosomes are relatively rigid hollow spheres with characteristic dimensions and morphologies that depend on leafhopper species. Nanomechanical mapping AFM is used to determine a characteristic compression modulus for brochosomes on the order of 1−3 GPa, which is consistent with crystalline proteins. Overall, this work provides an improved understanding of the structural and mechanical properties of leafhopper brochosomes using a new set of ML-based image classification tools that can be broadly applied to nanostructured biological materials.

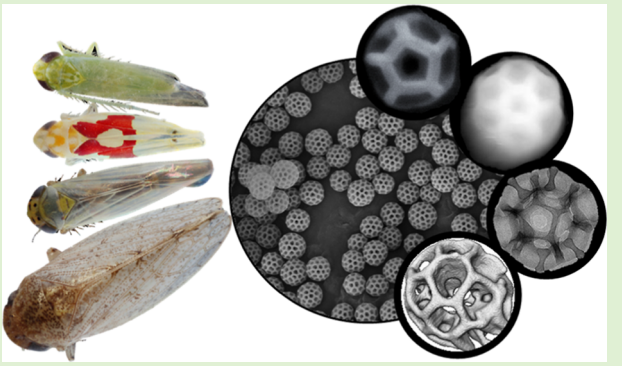

INTRODUCTION

Nature has evolved highly structured materials to aid the fitness and survival of animals and plants. In recent years, biological materials found in the earth's ecosystem have inspired the development of new functional materials for applications including optics,[1−5] acoustics,[6−8] tunable wettability,[9−15] and sensors.[16−19] Insects comprise nearly half of all known species of extant animals on earth[20,21] and have evolved multi-functional materials that often serve as an inspiration for the design of engineered materials.[22] For example, several species of butterflies and moths have developed nanoscale patterns that result in transparent wings and efficient transmission of light into optical sensors, which enables nocturnal sight due to impedance matching between the incident photons and nanostructures.[22,23] Cuticular adaptations have also evolved to support insect respiration and protection,[24] and these uniquely patterned exoskeletons have several functional roles for the insects that embody them.

In the early 1950s, Tulloch and Shapiro discovered that some subfamilies of insects known as leafhoppers produce highly ordered nanostructures resembling carbon-60 buckyballs with similar hexagonal and pentagonal geometric surface facets (Figure 1).[25,26] The sub-microscopic bodies were named "brochosomes" derived from the Greek words for the mesh of a net and body.[27] Subsequently, brochosomes were determined to be nanostructured entities composed of a combination of lipids and proteins, with some protein structures unique to brochosomes known as brochosomins.[28] Regarding the structural components of brochosomes, here, we refer to the primary brochosome features as pits, struts, and nodes, corresponding to hollow compartments, the walls of hollow compartments, and the intersection of compartment walls, respectively (Figure 1).

Brochosomes are produced by all major subfamilies of leafhoppers[29] and have been found as contaminants on both

Received: August 21, 2022
Revised: November 29, 2022
Published: December 14, 2022

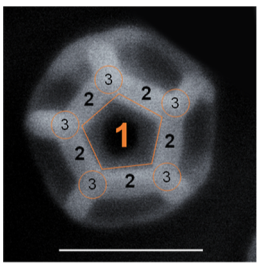

Figure 1. SEM image of brochosomes showing (1) pit, (2) strut, and (3) node structural features. Scale bar: 250 nm.

the integument of other insects[25,30] and in collected aerosol particles.[31−33] The superhydrophobic properties of leafhopper integuments resulting from brochosome coatings have been shown to protect leafhoppers from the contamination by their own sticky exudates,[34,35] thereby serving as an intrinsic non-stick coating on the insect body. In addition, the pitted brochosome morphology lends to strong omnidirectional anti-reflective properties for wavelengths between 250 and 2000 nm, which provides camouflage to leafhoppers and protects their eggs from potential predators.[1] The brochosome morphology is thought to govern their functional properties in nature,[1,34,36] which provides intriguing opportunities for materials design and engineering. The hollow hierarchical micro- and nanoscale structure of brochosomes, together with the reported morphology-driven properties of superhydrophobicity and anti-reflectivity, has motivated the design of brochosome-inspired synthetic particles.[1,36−38] Yang et al. recently reported metal, metal oxide, and polymeric artificial brochosomes with anti-reflective properties,[1] but the synthetic mimics are not hollow and do not exhibit the buckyball-like pentagonal and hexagonal face arrangement of natural brochosomes described above. Despite recent progress, synthetic brochosome mimics have not yet fully captured the intricate hierarchical structures of natural brochosomes.

Leafhoppers generally differ across species in their integumental patterning and size distribution, but the role of structural properties on functional behavior is not yet fully understood. In this work, we focus on understanding the structural properties of brochosomes from four distinct species of leafhoppers: *Curtara insularis*, *Macrosteles quadrilineatus*, *Eratoneura fulleri*, and *Empoasca* sp. (Figure 2). Due to the variability in the interspecies life history, several open questions remain regarding the morphogenesis, structure−function relationships, and chemical and physical properties of brochosomes.[39] To understand interspecies variations and quantitatively characterize the brochosome morphology, large data sets on the structural characteristics across species are required with robust statistics. Techniques such as X-ray scattering can be used to reveal characteristic structural length scales, but such data are generally obtained by ensemble averaging methods, which preclude the analysis of sub-populations and distributions in the underlying ensemble.[40,41] Conversely, microscopy-based characterization techniques such as scanning electron microscopy (SEM) and transmission electron microscopy (TEM) provide real-space images, thereby enabling quantitative determination of structural features and distributions in the ensemble. However, quantitative analysis of electron microscopy (EM) data for nanostructured materials generally relies on precise image segmentation. Traditionally, image segmentation is performed by setting intensity thresholds to distinguish features with a different contrast,[42,43] which has limited performance under high noise conditions and on features with complicated intensity profiles, especially for multiple component feature segmentation.[44] From this perspective, quantitative characterization of biological materials with nanoscale structures would greatly benefit from automated or machine learning (ML)-based image analysis techniques suitable for processing large and complex data sets.[44]

EM-based multimodal characterization studies have previously been used to visualize and quantify self-assembled structures due to intrinsic advantages in the nanoscale resolution and in situ imaging capabilities.[45] By combining EM with ML and image analysis methods, high-throughput analysis of large and heterogeneous sample image sets becomes possible. Importantly, the combination of these approaches introduces capabilities not traditionally associated with the typical length scales probed using EM-based methods. Multimodal approaches for characterizing three-dimensional (3-D) nanostructures have found utility in soft materials and biomaterials research for applications involving the block copolymer self-assembly,[46] structure of DNA and peptide assemblies,[47−50] and polymer structure and assembly.[51−53] In this work, we develop ML-based methods to characterize large and complex SEM image-based data sets for brochosomes across several different leafhopper species. A convolutional neural network (U-Net) is trained using SEM images with multiple output channels for the simultaneous segmentation of brochosome particles and structural features (pits) on their surfaces. In this way, the U-Net method achieves accurate segmentation results and facilitates the high-throughput capabilities of the computer-assisted image processing methods. ML-based methods are complemented by soft matter characterization techniques including electron tomography and atomic force microscopy (AFM). Electron tomography is used to understand the 3-D hierarchical structure of brochosomes, thereby revealing structural information with striking detail at a nanoscale resolution. We further use AFM fast force mapping (FFM) to determine the modulus and nanomechanical properties of brochosomes. Broadly, this work demonstrates how EM and ML-based techniques may be utilized to quantitatively understand brochosomes and other similarly

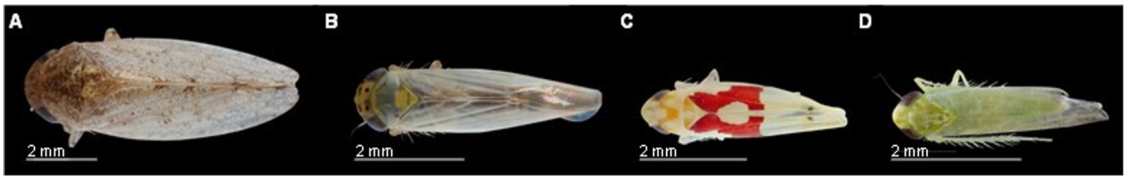

Figure 2. High-resolution optical images of four leafhopper species utilized in this work: (A) *C. insularis*, (B) *M. quadrilineatus*, (C) *E. fulleri*, and (D) *Empoasca* sp.

https://doi.org/10.1021/acs.biomac.2c01035
Biomacromolecules 2023, 24, 190−200

complex structures, which enables characterization of interspecies variation in the brochosome structure across four different leafhopper species.

MATERIALS AND METHODS

Leafhopper Collection, Identification, Rearing, and Measurement. Individual specimens of *C. insularis*, *Empoasca* sp., *E. fulleri*, and *M. quadrilineatus* were collected via sweep netting or through black light trapping from residential areas in central Illinois, USA. These leafhoppers were identified to genus or species using the 3I Interactive Keys and Taxonomic Databases.[54] All samples were caught live, frozen, and stored at −20 °C until examination and then allowed to air dry for at least 48 h at room temperature prior to experimental work. *C. insularis* and *M. quadrilineatus* specimens used to isolate brochosomes were obtained from populations maintained in the laboratory on barley at 22−25 °C with a 18L:6D photoperiod in Percival I-36LLVL environmental chambers (Perry, IA, USA). *M. quadrilineatus* was a gift from Nancy Moran (University of Texas at Austin) whose lab has maintained a long-term colony from leafhoppers collected in New Haven, CT. *C. insularis* were collected in Austin, TX, and its mitochondrial cytochrome oxidase subunit I (COI) barcode sequence was determined by sequencing the PCR product amplified using LepF and LepR primers[55] from DNA extracted using the DNeasy Blood & Tissue Kit (Qiagen). Querying the BOLD database[56] with this COI sequence returned a match to related Iassinae that led to species identification based on morphological traits. For all species, the body length was obtained by measuring the distance from the most proximal point of the head to the most distal tip of the forewing of three specimens per species using a micrometer. The mean of the three measurements from each species group was then calculated, and a representative member from each species was photographed.

Manual Method for Measuring Brochosome Dimensions. Leafhopper forewings were prepared for SEM by placing three forewings from three separate individual from each species dorsal side up on double-sided carbon conductive tape on aluminum SEM stubs. The forewings were sputter coated with a 7 nm layer of gold palladium (Au−Pd) using the Denton Desk II TSC turbo-pump sputter coater (Denton Vacuum, Inc., Moorestown, NJ, USA) in the Microscopy Suite, Imagining Technology Group, Beckman Institute for Advanced Science and Technology, UIUC. The proximal, medial, and distal portions of the forewings were imaged at 10,000×, 20,000×, or 30,000× magnifications using the Microscopy Suite's FEI Quanta FEG 450 environmental scanning electron microscope (ESEM) (Thermo Fisher Scientific Corp., Waltham, MA, USA) at a high vacuum setting, a low voltage of 5.0−10.00 kV, and a spot size of 3.0. For each species, two images per wing position (proximal, medial, or distal thirds in relation to the body) and three forewings per species were imaged for a total of at least 18 images per species. The diameter (nm) of the brochosomes were measured from these SEM images for each species using ImageJ Fiji version 2.3.0/1.53f software.[57] To account for the irregular shape of the brochosomes, the diameter measurements were taken at three different angles (0, 45, and 90°), and the mean was calculated to give a final diameter measurement. At least 40 brochosomes were measured per image and at least 420 brochosomes were measured per species. The total number of brochosomes measured exceeded 3900. The mean of these measurements was calculated per wing position and per species. A total of three individuals from each species were examined.

Brochosome Sample Preparation. A modified protocol[28] for the extraction of brochosomes from leafhoppers was executed by first immersing approximately 5−20 leafhoppers (larger leafhoppers require fewer specimens) in 20 mL of acetone for 15 min. The solution was then sonicated for 2−3 min at 40 kHz sonication frequency using a Branson 2510 ultrasonic cleaner. Care was taken to use low-power sonication so as to not destroy the leafhopper body. After the sonication, the solution was filtered through a Whatman 1 filter paper with light vacuum. The filtrate was collected and centrifuged at 20,000 rpm for 20 min. The supernatant was removed and checked for the absence of brochosome particulates, and fresh acetone was added before a performing a second centrifuge cycle. Finally, centrifuge vials were used to concentrate samples to generate a brochosome solution stock for further characterization.

Sample Preparation for EM. SEM samples were prepared by drop casting 40 μL of the brochosome stock solution onto a glass substrate and dried at room temperature under vacuum for roughly 12 h to remove as much solvent that may be pinned to or trapped within the brochosome structures. SEM was conducted on a FEI Quanta Field-Emission Gun 450 ESEM. Samples were sputter coated with roughly 7 nm of Au/Pd and imaged at 20 keV. Samples for TEM imaging were prepared using drop casting and solvent evaporation of roughly 10 μL of the brochosome stock solution onto carbon- and formvar-coated copper TEM grids, supplied by Ted Pella. Brochosome samples for electron tomography were prepared by following the same protocol as that of TEM sample preparation.

TEM Tomography. Transmission electron tomography was used to reconstruct the 3-D nanomorphology of brochosomes for the four different leafhopper species (Figure S1). The brochosomes selected fall within the size distributions expected for each leafhopper species (Figure S2). We measured these approximate brochosome diameters using the cross-sections of the tomographically reconstructed brochosomes (Figure S2A). The diameters for two brochosomes each of *Empoasca* sp., *E. fulleri*, *M. quadrilineatus*, and *C. insularis* calculated using reconstructed cross-sections are shown in Figure S2B. A comparison between the diameter distribution from ML and the diameter measured from reconstructed cross-sections is shown in Figure S2C. Ideally, the brochosomes selected would fall at the center of this distribution; however, several practical barriers associated with tomography render most brochosomes unfeasible for reconstruction. Using TEM tomography, we focused on isolated brochosome particles where possible, taking care to preserve the geometric surface structures. The brochosome samples were tilted along the *x*-axis to collect a series of 61 images. A low electron beam dose was maintained throughout the imaging process to minimize beam-induced damage to the biological specimen. The tilt projections were then combined to generate a tomogram, which was used for the 3-D reconstruction of the brochosome morphology (voxel size: 6.8 × 6.8 × 6.8 $Å^3$). Electron tomographic image reconstruction of brochosomes was performed using a JEOL 2100 Cryo TEM instrument at an acceleration voltage of 200 kV with the electron dose maintained at rate of 4−7 $e^- Å^{-2} s^{-1}$, a defocus value of −2048 nm, a tilt range of ±60°, and a tilt interval of 2°. Image processing, tomogram generation, and reconstructions were performed using IMOD 4.9.3[58] (http://bio3d.colorado.edu/), OpenMBIR[59] (https://engineering.purdue.edu/bouman/OpenMBIR/), and Amira 6.4 (Thermo Scientific). For tomogram denoising, three filtering modules were applied (median filter, Gaussian filter, and edge-preserving smoothing), followed by thresholding and smoothing modules. The ambient occlusion module was used for void reconstruction. The inner pore region was separated from the void volume using semi-manual segmentation, and the pits were segmented using watershed analysis.

AFM Preparation and Methods. AFM samples were prepared by drop casting several drops of a concentrated brochosome stock solution from acetone onto glass slides and drying under vacuum for several hours to minimize the trapped solvent. Traditional AFM topography and surface roughness measurements were conducted on an Asylum Cypher AFM instrument with Tap 300Al-G probes (force constant: 40 N/m and resonance frequency: 300 kHz). To study the mechanical properties of brochosomes, force−separation data were obtained using the FFM mode on an Asylum Research Cypher AFM instrument (Figure S6). Instead of using force−distance curves, which provide the distance as the position of the *z*-position sensor, force−separation data were used to provide the distance as the tip separation, which is the actual distance between the tip and the sample surface obtained by subtracting contributions from the cantilever deflection. Nanomechanical analysis and FFM force−distance plots of brochosomes were obtained using a CONTR contact mode AFM tip (force constant: 0.2 N/m and resonance frequency: 13

https://doi.org/10.1021/acs.biomac.2c01035
Biomacromolecules 2023, 24, 190−200

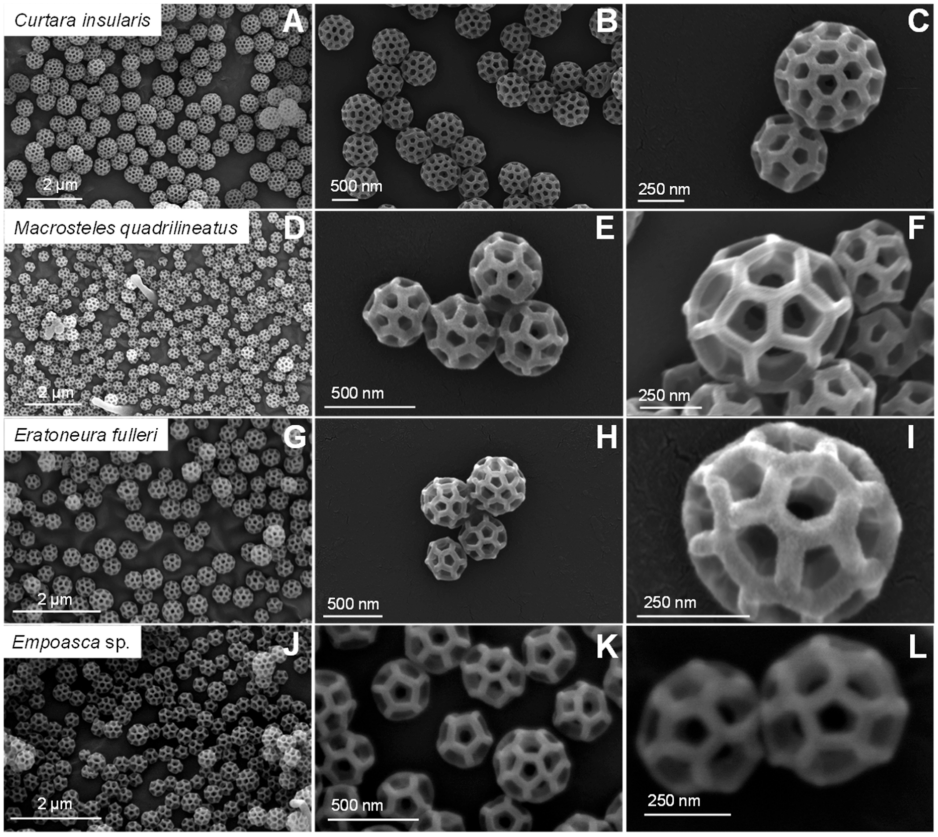

Figure 3. SEM images of brochosomes collected from (A–C) *C. insularis*, (D–F) *M. quadrilineatus*, (G–I) *E. fulleri*, and *Empoasca* sp. (J–L). Lower-magnification images (A,D,G,J) show relative distributions of brochosomes on the surfaces of leafhoppers cuticles. Intermediate-magnification images (B,E,H,K) show heterogeneity of types of brochosomes present in each distribution. High-magnification images (C,F,I,L) show detailed structural characteristics of brochosomes.

kHz). The spring constant range of 0.02–0.77 N/m was reported by the manufacturer of the AFM contact probe, and an independent internal calibration was performed using the Asylum Cypher GetReal software during each experiment, confirming the spring constant values for all probes to be between 0.53 and 0.69 N/m. To study whether force spectroscopy measurements differed within a single brochosome or across multiple brochosomes, five regions on each brochosome were randomly selected for analysis. An average force–separation curve containing the five chosen points was obtained for each of the four brochosomes. To obtain force measurements, the deflection was converted to force using Hooke's Law = $-kx$, where x is the change in the piezo height and k is the spring constant of the cantilever. Collectively, the four average force–separation curves were analyzed to determine the modulus, adhesion, and deformation properties of brochosomes.

RESULTS AND DISCUSSION

EM and Electron Tomography of Brochosomes. We began by using SEM imaging to characterize the structure of brochosomes from four different leafhopper species including *C. insularis*, *M. quadrilineatus*, *E. fulleri*, and *Empoasca* sp. High-throughput image analysis for SEM typically relies on intensity thresholding-based binarization;[40,43] however, the complex structure of brochosomes including nanoscale pits and struts (Figure 1) leads to complexities in intensity profiles, which precludes simple intensity thresholding of images. Prior work used SEM to determine the brochosome structure,[28,34,35] including direct visualization of the surface morphology and characterization of the internal structure by fracturing brochosomes trapped in a polymer matrix, but this method only provided a cross-sectional view of the internal morphology.[34] In this work, we directly quantify strut and pit morphologies from the brochosome surface to the interior, which requires detailed segmentation of brochosome surfaces.

Brochosome images were collected from four species of leafhopper (Figure 3) at lower magnifications to show the particle distributions on the insect cuticles (Figure 3A,B,D,E,G,H,J,K) and at higher magnifications to visualize nanoscale structures (Figure 3C,F,I,L). Our results show that brochosomes from these different species adopt a regular buckyball-like morphology with dihedral tessellations and seemingly hollow structures based on images shown in Figure 3F, where the substrate appears to be visible through brochosome pits. SEM images show that the dihedral tessellations of brochosomes organize as pentagons and hexagons, and the number of pentagons and hexagons depends on the brochosome diameter and the number of pits present on the brochosome surface. *C. insularis* is the largest leafhopper species studied here with an average adult body length of 7.9 ± 0.3 mm (SD) (N = 3); brochosomes from *C. insularis* have the largest diameters compared to brochosomes from the *Macrosteles*, *Eratoneura*, and *Empoasca* species, which are generally smaller. The average brochosome diameter observed through manual measurements ranged from approximately 410.2 ± 51.5 nm (SD) (N = 500) for *E. fulleri* to 685 ± 66.8 nm (SD) (N = 360) for the *C. insularis*. Although SEM images indicate that brochosomes appear to adopt a hollow internal structure, we used additional imaging methods to fully characterize the surface features and internal structures of brochosomes.

https://doi.org/10.1021/acs.biomac.2c01035
Biomacromolecules 2023, 24, 190–200

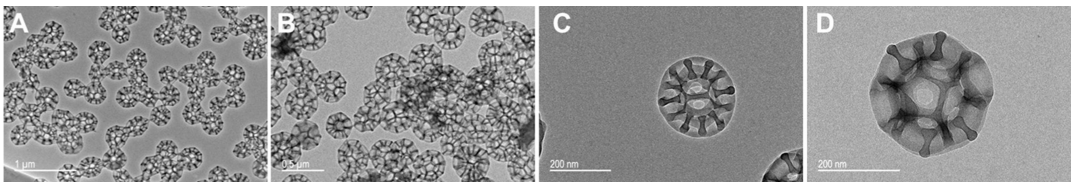

Figure 4. TEM images of brochosomes from *Empoasca* sp. show that brochosome structures are electron beam stable. (A,B) TEM images showing the distribution of brochosomes drop cast from solution. (C,D) Isolated, intact brochosome images using TEM.

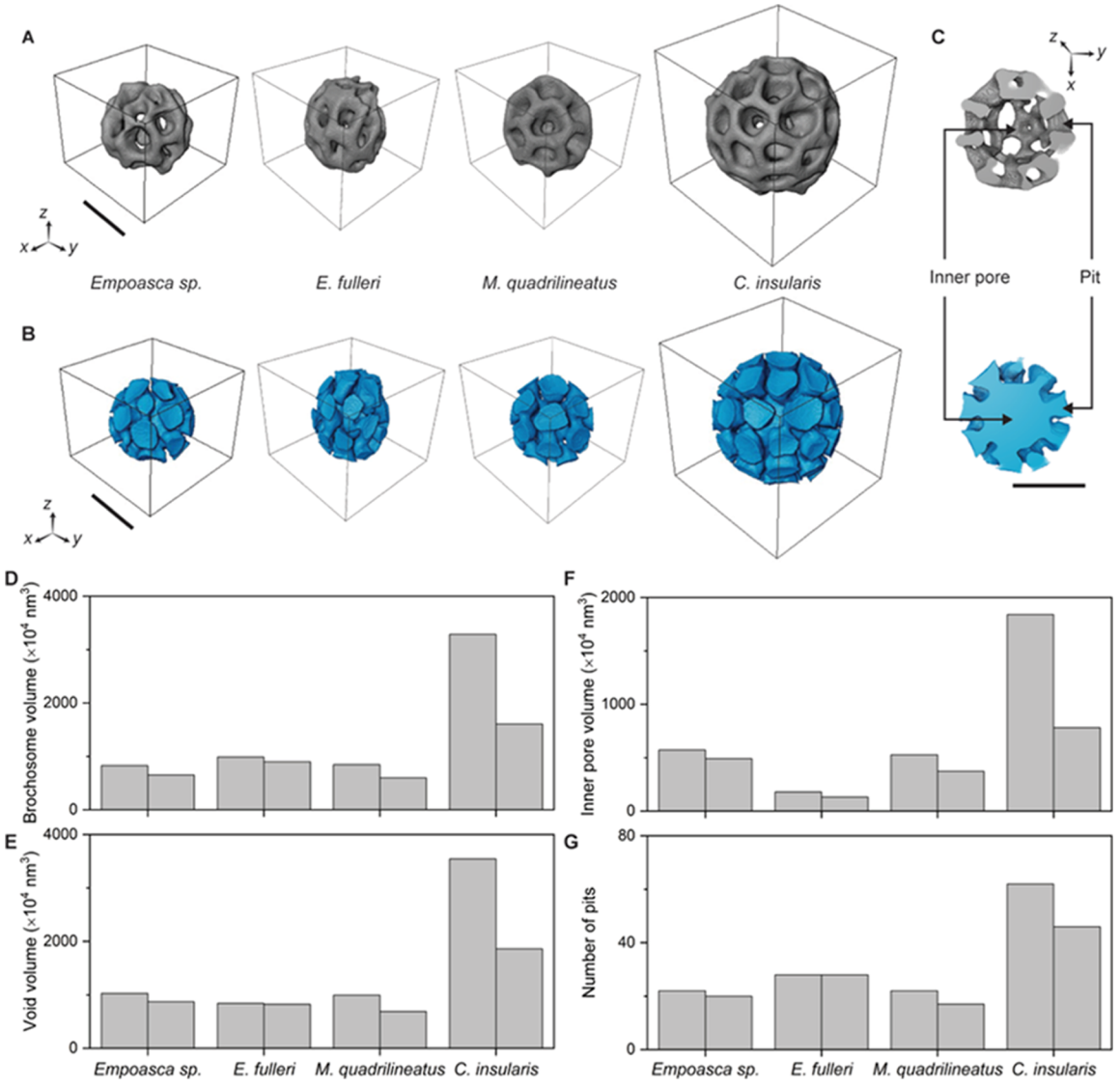

Figure 5. Electron tomographic reconstructions of brochosomes. (A) 3-D reconstructions of representative brochosomes of *Empoasca* sp., *E. fulleri*, *M. quadrilineatus*, and *C. insularis* (left to right). (B) Corresponding void reconstructions of the brochosomes in (A). (C) Cross-section of the brochosome material and void reconstructions showing the internal void structure with the inner pore region and pit channels. Brochosome volume (D) void volume (E) inner pore volume (F) parameters, and number of pits (G) of brochosomes showing the correlation between the brochosome volume and the total void volume, inner pore volume, and number of pits. Scale bars: 250 nm.

TEM imaging was used to determine the electron beam stability of brochosomes and to characterize brochosome clustering (Figure 4). TEM images in Figure 4A,B show that some brochosomes may adhere to others across a large area of brochosomes. We note that brochosome samples imaged directly on leafhopper cuticles also show interparticle interactions (Figure S1), which suggests that sample processing for TEM imaging does not give rise to the observed clustering interactions. Leafhopper cuticles are well-documented to be coated in waxes, and the presence of waxes on particle boundaries could give rise to the observed brochosome adhesion.[60] Two isolated brochosomes with different strut orientations are shown in Figure 4C,D.

To understand the internal pore structure, we performed full 3-D tomographic reconstructions of brochosomes from the four different leafhopper species (Figures 5A, S3, and S4). We observe a mixture of nearly spherical, isolated, and conjoined brochosomes. Analogous to SEM images, results from TEM

https://doi.org/10.1021/acs.biomac.2c01035
Biomacromolecules 2023, 24, 190−200

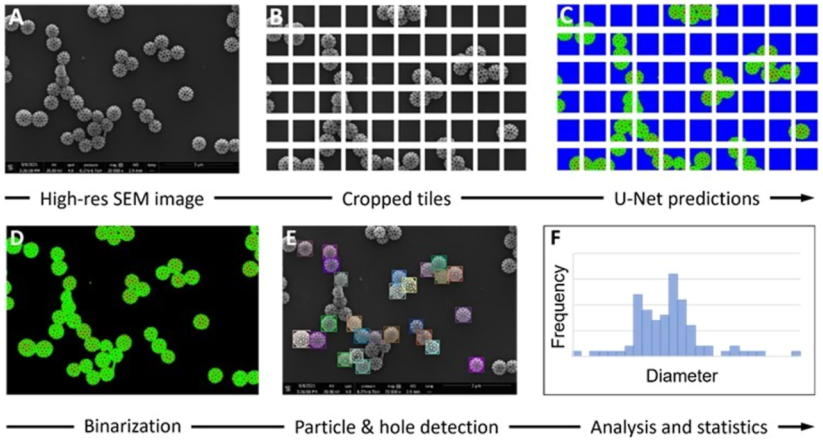

Figure 6. Workflow showing the process for 2-D image analysis and processing of high-resolution SEM images of *C. insularis* brochosomes. (A) Original high-resolution SEM images. (B) Cropped tiles for the original SEM image. (C) U-Net predictions and segmentation of images. (D) Binarization of images. (E) Particle and hole detection. (F) Analysis and statistics of the specimen.

tomography show a tessellated surface structure consisting of pentagonal and hexagonal faces and hollow pit channels extending to the brochosome core. Electron tomography thus enables the visualization of the 3-D structure of brochosomes and further allows for quantitative morphometric measurements of the 3-D reconstructed images. In this way, we quantified the volume of brochosomes, with *Empoasca* sp., *E. fulleri*, *M. quadrilineatus*, and *C. insularis* having brochosome volumes of 8.3×10^6, 9.9×10^6, 8.4×10^6, and 16.1×10^6 nm,[3] respectively (Table S1). Slice-by-slice cross-sections clearly show an intricate internal void structure in the brochosome interior (Movie S1).

Recent work used computational modeling to study brochosome-inspired metal−dielectric composite materials,[61] wherein plasmonic metals were used to model the brochosome structure and internal voids were modeled as dielectric materials. Computational results on synthetic brochosomes revealed interesting optical properties such as metamaterial behavior,[61] which suggests that brochosome materials and internal void structures play a key role in determining functional properties. Based on these results, we implemented a reconstruction module to artificially fill the void volume space (Materials and Methods), allowing us to visualize the 3-D morphology of brochosome voids. Figure 5B shows the volume-filled reconstructions of the brochosome voids, where *Empoasca* sp., *E. fulleri*, *M. quadrilineatus*, and *C. insularis* have void volumes of 10.3×10^6, 8.3×10^6, 10.0×10^6, and 18.6×10^6 nm,[3] respectively (Table S1). Reconstructed 3-D images from TEM tomography (Figure 5C) clearly show that the interior structure of brochosomes is hollow and reveal the nature of internal pit-formed channels. Prior work reporting the brochosome internal structure relied on destructive shearing of the brochosome into fragments, which could alter the native brochosome structure.[34] Furthermore, brochosome cross-sections reveal two distinct regions within the void, including a nearly spherical hollow inner core and channel-like pits connected to the inner core (Figure 5C). The reconstructed void volume is used to segment the inner pore and pit regions for morphometric measurements (Figure S5 and Movie S2).

Unlike TEM and SEM micrographs, tomographic reconstruction captures the complete 3-D structure of a nanomaterial. Void segmentation allows for quantifying the total number of pit channels for brochosomes, thereby enabling the correlation of brochosome size with the number of pits. Our results show that as the brochosome volume decreases, the total void volume, inner pore volume, and number of pits decrease for brochosomes across all four species (Figure 5D−G and Table S1). These results suggest that 3-D electron tomographic reconstruction can be used to gain new insights regarding brochosome morphogenesis. Specifically, for processes where structural features may be synthetically controlled using geometrically confined or phase-separation-driven molecular assembly, such characteristics may be tuned according to their structure−property implications. In this way, the biological observations reported in this work serve as a guide for the design of synthetic materials. Based on the 3-D image reconstructions, our results show that brochosomes exhibit morphological variations between species and further show variations within the same species. Nevertheless, although our electron tomography workflow has allowed us to access morphometric measurements, it generally lacks the ability to perform bulk analysis, which may be useful in characterizing polydisperse and polymorphous systems. Thus, the tomographic analysis was complemented with bulk analysis using two-dimensional (2-D) ML-based methods.

ML-Based Image Analysis of Brochosomes. High-resolution SEM images were further used for 2-D image analysis of brochosomes collected from different leafhopper species. Here, we used an ML-based algorithm known as U-Net for SEM image segmentation of brochosomes. U-Net was recently used to identify nanoparticles from EM images[62] and allows for high-throughput image analysis with sufficient statistical significance and precision to quantify brochosome surface and pit structures. High-resolution SEM images are first cropped into tiles to match the input size of the U-Net model without scaling, which could result in a decrease in the spatial resolution (Figure 6A,B). Next, our U-Net model treats the image segmentation as a 3-class pixelwise classification problem to distinguish the brochosome and the pit from the background (Figure 6B), which is challenging using conventional thresholding-based segmentation methods due to complex image contrast profiles. We further discuss a comparison of these thresholding methods in Figure S8. Segmented, binary images representing individual brochosomes and their corresponding pits are then stitched back

https://doi.org/10.1021/acs.biomac.2c01035
Biomacromolecules 2023, 24, 190−200

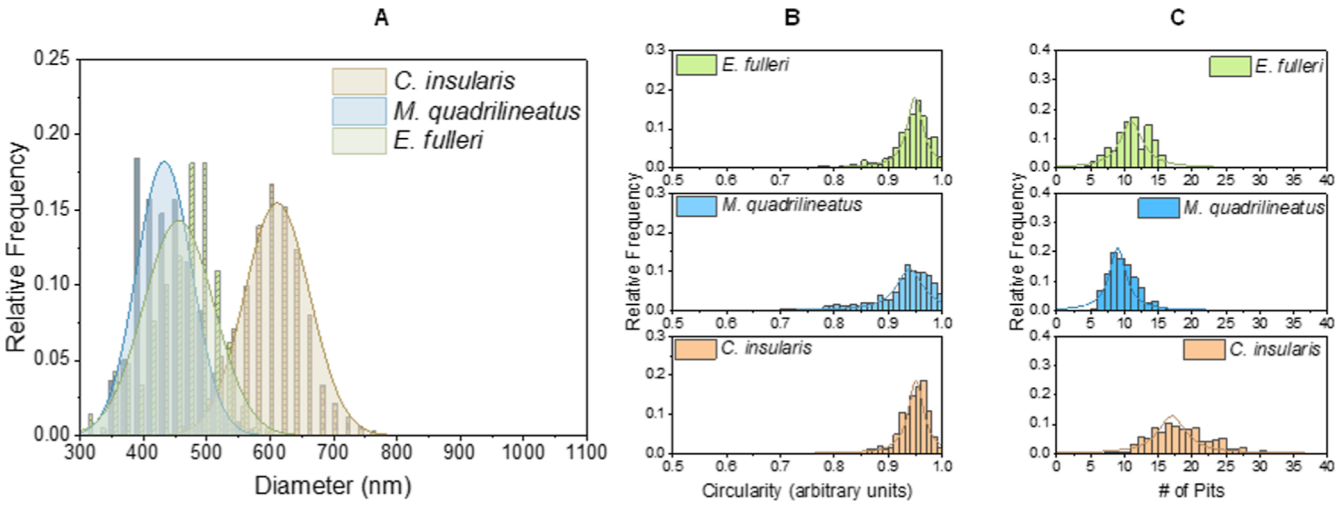

Figure 7. Statistical analysis histograms of brochosome structural characteristics across different species of leafhoppers. Histograms showing the distribution of the brochosome (A) diameter, (B) circularity, and (C) number of pits.

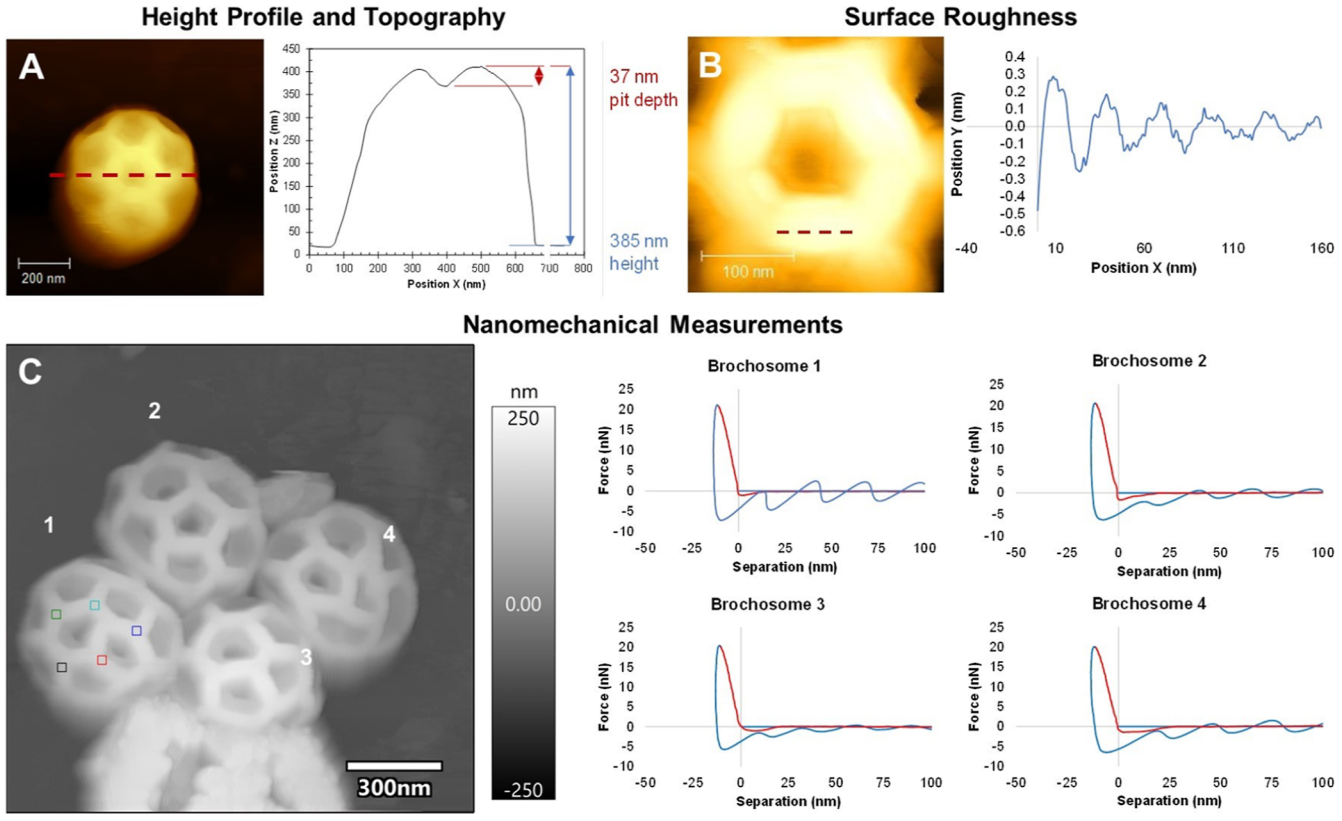

Figure 8. AFM imaging analysis of brochosomes from *Empoasca* sp. including structural characteristics and FFM for nanomechanical properties. (A) Height profile and surface topography, (B) surface roughness of the brochosome axis, and (C) nanomechanical measurements of four brochosomes in a single AFM image and force−separation curves for each brochosome used for quantitative analysis of mechanical properties. Red and blue lines in nanomechanical analysis refer to approach and retract curves, respectively.

together and analyzed by conventional algorithms to determine structural descriptors such as the area, diameter, circularity, eccentricity, solidity, centroid position, and number of pits per brochosome (Figure 6D,E). Unlike previously reported computational models[44,63] or rendering software,[62] U-Net requires only a small number of manually curated experimental images (25 out of 4224) to serve as the training data set, which are augmented through random combinations of rotating, zooming, and flipping. Overall, these results highlight the flexibility of the U-Net ML-based algorithm for analyzing experimentally determined SEM images from ordered biomaterials. To note, U-Net feature segmentation is a viable method for structural analysis regardless of whether the shapes of the features of interest are spherical. For example, U-Net has been used to detect gold nanoparticles with triangular, square, and rod-like shape under TEM.[44]

After the ML algorithm was trained and executed, a series of structural features and descriptors for brochosomes were

https://doi.org/10.1021/acs.biomac.2c01035
Biomacromolecules 2023, 24, 190−200

Table 1. Brochosome Moduli Determined from AFM−FFM from Four Species of Leafhoppers

species	brochosome 1 modulus (GPa)	brochosome 2 modulus (GPa)	brochosome 3 modulus (GPa)	brochosome 4 modulus (GPa)	average brochosome modulus (GPa)
C. insularis	0.86	1.02	2.26	3.66	1.95
M. quadrilineatus	1.11	1.16	1.67	1.81	1.44
E. fulleri	0.74	0.87	1.09	1.79	1.12
Empoasca	0.77	0.81	1.19	2.90	1.42

determined for each species of leafhopper (Figure 7). Results from the ML algorithm show that *C. insularis* (N = 323) has the largest brochosome diameters, which averaged 611 ± 52 nm standard deviation, whereas *M. quadrilineatus* (N = 217) and *E. fulleri* (N = 213) have average diameters of 433 ± 44 nm and 455 ± 56 nm, respectively. In addition, average brochosome size (diameter) measurements were also performed manually by averaging three measurements of each brochosome at three separate angles (0, 45, and 90°) to account for imperfect circularity, as demonstrated in Figure 7B. In this way, automated size measurements from ML-based analysis were compared to manually determined diameter measurements for *C. insularis* (N = 360), *M. quadrilineatus* (N = 540), and *E. fulleri* (N = 500), where diameters were manually determined from SEM images by averaging three diameter measurements of each brochosome at three separate angles as mentioned above. The automated diameter measurements for all three species were found to be within 0.5−2.5% of the manually collected diameter measurements and thus indistinguishable from the manual analysis method.

We further determined the circularity of brochosomes, which is a parameter that describes how close 2-D projections of the brochosomes are to circular shapes, where a value of 1.0 corresponds to a perfect circle (Figure 7B and eq S1). Circularity may be used as an indicator of brochosome deformation, albeit naturally occurring deformation or processing-induced deformation. In addition, the U-Net method was also used to determine the number of pits on the surface of each brochosome in 2-D projected images. However, such measurements are inherently limited by viewing a 3-D structure in a 2-D image, such that only a single side of the brochosome is visible in the initial image. Nevertheless, ML-based image data are obtained on the timescale of minutes compared to manual data collection and analysis, which generally required several weeks for analysis. From this view, ML-based methods enable robust quantification of brochosome features across several leafhopper species by increasing the statistical power of data collection and streamlining particle image analysis. Our use of these developed image analysis tools to analyze brochosome tessellations is included in Figure S7.

AFM and Mechanical Properties of Brochosomes. AFM provides a useful method for the nondestructive mechanical characterization of materials.[64] AFM nanomechanical mapping allows for localized property measurements with a nanoscale spatial resolution for analyzing soft materials,[65] including polymers, proteins, cells, and biopolymers with elastic moduli on the order of 100 Pa to 10 GPa. Here, we used AFM to determine the nanomechanical properties of brochosomes from four leafhopper species (Figure 8). Height profiles determined from AFM measurements show a characteristic brochosome particle from *Empoasca* sp. with a height of 385 nm and pit depths of 37 nm (Figure 8A). An average surface roughness, R_a, was determined across a single strut of the same brochosome and was found to be R_a = 277 pm, which indicates that brochosome strut surfaces are smooth.

FFM nanomechanical analysis revealed that brochosomes are relatively hard biological particles with low surface adhesion. By determining the slope of the approach line and applying the Hertzian model for a four-sided pyramid based on the AFM cantilever tip geometry, the compression modulus K was determined for brochosomes from all four species (Table 1 and Figure S6).

As a point of structural comparison, compression moduli values for brochosomes are in alignment with reported moduli values of crystalline proteins, which have been shown in other reports to be a part of the brochosome structure.[28,66,67] It is important to notes that the referenced proteins may not be identical in structure or 3-D architecture to our brochosome proteins; however, based on the length scale of our nanomechanical measurements (<8 nm AFM probe), it is more likely that the modulus values that we have measured are closer to that of the protein aggregates than the modulus associated with the composite nanostructured architecture of the whole brochosome. As a result, no significant correlations have been observed between the brochosome nanostructure and resulting compression modulus. In addition, the force−separation curves show that the brochosomes exhibit plastic deformation characteristics, which suggests that after the AFM tip has retracted from the surface of the brochosome, the surface does not return to its original state. The mechanical measurements also allow for the determination of the adhesive force, which is related to the cantilever deflection during tip retraction and is indicative of adhesion between the brochosome surface and the AFM probe. The larger the adhesive force of the sample, the more dramatic the bend in the cantilever, which results in a deeper minimum in the retraction curve. The adhesive force for each of the four brochosomes was determined by taking the difference between the x-axis and the minimum value of the retraction curve, and the average adhesion force of the four brochosomes was found to be 6.4 ± 0.6 nN. The relatively weak adhesive characteristics of brochosomes is attributed to the protein−lipid chemical composition of brochosomes and is similar to the weak adhesive characteristics of ferritin and bovine serum albumin to hydrophilic substrates.[68,69]

CONCLUSIONS

In this work, electron tomography is used to provide a full 3-D analysis of the brochosome structure, and ML-based methods are coupled with high-resolution 2-D imaging to quantitatively understand brochosome characteristics across leafhopper species. AFM methods are further used to determine the compression modulus and mechanical properties of free-standing leafhopper brochosomes. Our results show that brochosomes are highly ordered, relatively hard, and inelastic 3-D structures with dihedral tessellated pits that form channels to a central hollow core. The complex morphology of

https://doi.org/10.1021/acs.biomac.2c01035
Biomacromolecules 2023, 24, 190−200

brochosomes required the use of ML-based methods to effectively identify and segment brochosomes from high-resolution SEM images, which further enables large-scale analysis of brochosome characteristics across leafhopper species. Compression modulus values for brochosomes are consistent with those of crystalline proteins. Our work provides an improved understanding of the structural characteristics of brochosomes that will be useful informing the functional roles of leafhopper brochosomes in nature.[34,35,39,70] Broadly, our findings contribute to an emerging body of work that aims to elucidate the functional properties and capabilities of brochosome particles while further providing evidence to support other structure−function hypotheses for brochosomes. In addition, the nanoscale characterization and ML-based analysis methods developed in this work hold the potential to link the structure of brochosomes to their natural functions and could inspire the development of new synthetic brochosome mimics with desired functionalities. Broadly, we envision that the methods developed in this work will be useful in characterizing a wide range of nanomaterials and hierarchically structured biomaterials beyond leafhopper brochosomes.

■ ASSOCIATED CONTENT

Supporting Information

The Supporting Information is available free of charge at https://pubs.acs.org/doi/10.1021/acs.biomac.2c01035.

SEM of brochosomes on the leafhopper cuticle with signs of cuticular wax and disfigurement; TEM images at zero tilt used for tomographic reconstruction; material and void volume from TEM tomographic reconstructions; morphometric volume parameters calculated for brochosomes; segmented brochosome pore void; circularity parameter and quantitative analysis; and nanomechanical analysis of brochosomes from four different leafhopper species (PDF)

Material and void sliced cross-sections of brochosomes from *Empoasca* sp., *E. fulleri*, *M. quadrilineatus*, and *C. insularis* (MP4)

Segmented pits of the *Empoasca* sp. brochosome void reconstruction (AVI)

■ AUTHOR INFORMATION

Corresponding Author

Charles M. Schroeder − *Department of Materials Science and Engineering, University of Illinois at Urbana-Champaign, Champaign, Illinois 61801, United States; Beckman Institute for Advanced Science and Technology and Department of Chemical and Biomolecular Engineering, University of Illinois at Urbana-Champaign, Champaign, Illinois 61801, United States;* orcid.org/0000-0001-6023-2274; Email: cms@illinois.edu

Authors

Gabriel R. Burks − *Department of Materials Science and Engineering, University of Illinois at Urbana-Champaign, Champaign, Illinois 61801, United States; Beckman Institute for Advanced Science and Technology, University of Illinois at Urbana-Champaign, Champaign, Illinois 61801, United States;* orcid.org/0000-0003-0985-0450

Lehan Yao − *Department of Materials Science and Engineering, University of Illinois at Urbana-Champaign, Champaign, Illinois 61801, United States;* orcid.org/0000-0003-1945-833X

Falon C. Kalutantirige − *Department of Chemistry, University of Illinois at Urbana-Champaign, Champaign, Illinois 61801, United States*

Kyle J. Gray − *Beckman Institute for Advanced Science and Technology and Department of Chemical and Biomolecular Engineering, University of Illinois at Urbana-Champaign, Champaign, Illinois 61801, United States*

Elizabeth Bello − *Beckman Institute for Advanced Science and Technology and Department of Entomology, University of Illinois at Urbana-Champaign, Champaign, Illinois 61801, United States*

Shreyas Rajagopalan − *Beckman Institute for Advanced Science and Technology and Department of Entomology, University of Illinois at Urbana-Champaign, Champaign, Illinois 61801, United States*

Sarah B. Bialik − *Department of Molecular Biosciences, The University of Texas at Austin, Austin, Texas 78712, United States*

Jeffrey E. Barrick − *Department of Molecular Biosciences, The University of Texas at Austin, Austin, Texas 78712, United States;* orcid.org/0000-0003-0888-7358

Marianne Alleyne − *Beckman Institute for Advanced Science and Technology, Department of Entomology, and Department of Mechanical Science and Engineering, University of Illinois at Urbana-Champaign, Champaign, Illinois 61801, United States*

Qian Chen − *Department of Materials Science and Engineering, University of Illinois at Urbana-Champaign, Champaign, Illinois 61801, United States; Beckman Institute for Advanced Science and Technology, Department of Chemistry, and Department of Chemical and Biomolecular Engineering, University of Illinois at Urbana-Champaign, Champaign, Illinois 61801, United States;* orcid.org/0000-0002-1968-441X

Complete contact information is available at: https://pubs.acs.org/10.1021/acs.biomac.2c01035

Notes

The authors declare no competing financial interest.

■ ACKNOWLEDGMENTS

This work was supported by a Multidisciplinary University Research Initiative (MURI) grant from the Army Research Office (W911NF-20-1-0195) for J.E.B., C.M.S., G.R.B., and K.J.G. E.B. was supported by a Beckman Graduate Student Fellowship. The development of ML algorithms and analysis of EM images were supported by the US Department of Energy, Office of Basic Energy Sciences, Division of Materials Sciences and Engineering, under award DE-SC0020723 (L.Y. and Q.C.). We acknowledge the Central Research Facilities in the Illinois Materials Research Laboratory (MRL) and the Beckman Institute for Advanced Science and Technology at the University of Illinois at Urbana-Champaign.

■ REFERENCES

(1) Yang, S.; Sun, N.; Stogin, B. B.; Wang, J.; Huang, Y.; Wong, T.-S. Ultra-Antireflective Synthetic Brochosomes. *Nat. Commun.* **2017**, *8*, 1285.

(2) Ding, Q.; Kang, Y.; Li, W.; Sun, G.; Liu, H.; Li, M.; Ye, Z.; Zhou, M.; Zhou, J.; Yang, S. Bioinspired Brochosomes as Broadband and

Omnidirectional Surface-Enhanced Raman Scattering Substrates. *J. Phys. Chem. Lett.* **2019**, *10*, 6484−6491.
(3) Tadepalli, S.; Slocik, J. M.; Gupta, M. K.; Naik, R. R.; Singamaneni, S. Bio-Optics and Bio-Inspired Optical Materials. *Chem. Rev.* **2017**, *117*, 12705−12763.
(4) Xiao, M.; Shawkey, M. D.; Dhinojwala, A. Bioinspired Melanin-based Optically Active Materials. *Adv. Opt. Mater.* **2020**, *8*, 2000932.
(5) Jin, Y.; Tai, H.; Hiltner, A.; Baer, E.; Shirk, J. S. New Class of Bioinspired Lenses with a Gradient Refractive Index. *J. Appl. Polym. Sci.* **2007**, *103*, 1834−1841.
(6) Dong, E.; Song, Z.; Zhang, Y.; Ghaffari Mosanenzadeh, S. G.; He, Q.; Zhao, X.; Fang, N. X. Bioinspired Metagel with Broadband Tunable Impedance Matching. *Sci. Adv.* **2020**, *6*, No. eabb3641.
(7) Dinh Le, T.-S.; An, J.; Huang, Y.; Vo, Q.; Boonruangkan, J.; Tran, T.; Kim, S.-W.; Sun, G.; Kim, Y.-J. Ultrasensitive Anti-Interference Voice Recognition by Bio-Inspired Skin-Attachable Self-Cleaning Acoustic Sensors. *ACS Nano* **2019**, *13*, 13293−13303.
(8) Wilmott, D.; Alves, F.; Karunasiri, G. Bio-Inspired Miniature Direction Finding Acoustic Sensor. *Sci. Rep.* **2016**, *6*, 29957.
(9) Oh, J.; Dana, C. E.; Hong, S.; Román, J. K.; Jo, K. D.; Hong, J. W.; Nguyen, J.; Cropek, D. M.; Alleyne, M.; Miljkovic, N. Exploring the Role of Habitat on the Wettability of Cicada Wings. *ACS Appl. Mater. Interfaces* **2017**, *9*, 27173−27184.
(10) Oh, J.; Hoffman, J. B.; Hong, S.; Jo, K. D.; Román-Kustas, J.; Reed, J. H.; Dana, C. E.; Cropek, D. M.; Alleyne, M.; Miljkovic, N. Dissolvable Template Nanoimprint Lithography: A Facile and Versatile Nanoscale Replication Technique. *Nano Lett.* **2020**, *20*, 6989−6997.
(11) Liu, K.; Jiang, L. Bio-Inspired Design of Multiscale Structures for Function Integration. *Nano Today* **2011**, *6*, 155−175.
(12) Park, K.-C.; Kim, P.; Grinthal, A.; He, N.; Fox, D.; Weaver, J. C.; Aizenberg, J. Condensation on Slippery Asymmetric Bumps. *Nature* **2016**, *531*, 78−82.
(13) Nguyen, S. H.; Webb, H. K.; Mahon, P. J.; Crawford, R. J.; Ivanova, E. P. Natural Insect and Plant Micro-/Nanostructsured Surfaces: An Excellent Selection of Valuable Templates with Superhydrophobic and Self-Cleaning Properties. *Molecules* **2014**, *19*, 13614−13630.
(14) Deparis, O.; Mouchet, S.; Dellieu, L.; Colomer, J.-F.; Sarrazin, M. Nanostructured Surfaces: Bioinspiration for Transparency, Coloration and Wettability. *Mater. Today: Proc.* **2014**, *1*, 122−129.
(15) Agonafer, D. D.; Lee, H.; Vasquez, P. A.; Won, Y.; Jung, K. W.; Lingamneni, S.; Ma, B.; Shan, L.; Shuai, S.; Du, Z.; Maitra, T.; Palko, J. W.; Goodson, K. E. Porous Micropillar Structures for Retaining Low Surface Tension Liquids. *J. Colloid Interface Sci.* **2018**, *514*, 316−327.
(16) Suresh Kumar, N.; Padma Suvarna, R.; Chandra Babu Naidu, K.; Banerjee, P.; Ratnamala, A.; Manjunatha, H. A Review on Biological and Biomimetic Materials and Their Applications. *Appl. Phys. A* **2020**, *126*, 445.
(17) Lee, B.-Y.; Kim, J.; Kim, H.; Kim, C.; Lee, S.-D. Low-Cost Flexible Pressure Sensor Based on Dielectric Elastomer Film with Micro-Pores. *Sens. Actuators, A* **2016**, *240*, 103−109.
(18) Ha, M.; Lim, S.; Park, J.; Um, D.; Lee, Y.; Ko, H. Bioinspired Interlocked and Hierarchical Design of ZnO Nanowire Arrays for Static and Dynamic Pressure-sensitive Electronic Skins. *Adv. Funct. Mater.* **2015**, *25*, 2841−2849.
(19) Shi, R.; Lou, Z.; Chen, S.; Shen, G. Flexible and Transparent Capacitive Pressure Sensor with Patterned Microstructured Composite Rubber Dielectric for Wearable Touch Keyboard Application. *Sci. China Mater.* **2018**, *61*, 1587−1595.
(20) Bar-On, Y. M.; Phillips, R.; Milo, R. The Biomass Distribution on Earth. *Proc. Natl. Acad. Sci. U.S.A.* **2018**, *115*, 6506−6511.
(21) Misof, B.; Liu, S.; Meusemann, K.; Peters, R. S.; Donath, A.; Mayer, C.; Frandsen, P. B.; Ware, J.; Flouri, T.; Beutel, R. G.; Niehuis, O.; Petersen, M.; Izquierdo-Carrasco, F.; Wappler, T.; Rust, J.; Aberer, A. J.; Aspöck, U.; Aspöck, H.; Bartel, D.; Blanke, A.; Berger, S.; Böhm, A.; Buckley, T. R.; Calcott, B.; Chen, J.; Friedrich, F.; Fukui, M.; Fujita, M.; Greve, C.; Grobe, P.; Gu, S.; Huang, Y.; Jermiin, L. S.; Kawahara, A. Y.; Krogmann, L.; Kubiak, M.; Lanfear, R.; Letsch, H.; Li, Y.; Li, Z.; Li, J.; Lu, H.; Machida, R.; Mashimo, Y.; Kapli, P.; McKenna, D. D.; Meng, G.; Nakagaki, Y.; Navarrete-Heredia, J. L.; Ott, M.; Ou, Y.; Pass, G.; Podsiadlowski, L.; Pohl, H.; von Reumont, B. M.; Schütte, K.; Sekiya, K.; Shimizu, S.; Slipinski, A.; Stamatakis, A.; Song, W.; Su, X.; Szucsich, N. U.; Tan, M.; Tan, X.; Tang, M.; Tang, J.; Timelthaler, G.; Tomizuka, S.; Trautwein, M.; Tong, X.; Uchifune, T.; Walzl, M. G.; Wiegmann, B. M.; Wilbrandt, J.; Wipfler, B.; Wong, T. K.; Wu, Q.; Wu, G.; Xie, Y.; Yang, S.; Yang, Q.; Yeates, D. K.; Yoshizawa, K.; Zhang, Q.; Zhang, R.; Zhang, W.; Zhang, Y.; Zhao, J.; Zhou, C.; Zhou, L.; Ziesmann, T.; Zou, S.; Li, Y.; Xu, X.; Zhang, Y.; Yang, H.; Wang, J.; Wang, J.; Kjer, K. M.; Zhou, X. Phylogenomics Resolves the Timing and Pattern of Insect Evolution. *Science* **2014**, *346*, 763−767.
(22) Schroeder, T. B. H.; Houghtaling, J.; Wilts, B. D.; Mayer, M. It's Not a Bug, It's a Feature: Functional Materials in Insects. *Adv. Mater.* **2018**, *30*, 1705322.
(23) Siddique, R. H.; Gomard, G.; Hölscher, H. The Role of Random Nanostructures for the Omnidirectional Anti-Reflection Properties of the Glasswing Butterfly. *Nat. Commun.* **2015**, *6*, 6909.
(24) Nickerl, J.; Helbig, R.; Schulz, H.-J.; Werner, C.; Neinhuis, C. Diversity and Potential Correlations to the Function of Collembola Cuticle Structures. *Zoomorphology* **2013**, *132*, 183−195.
(25) Tulloch, G. S.; Shapiro, J. E.; Cochran, G. W. The Occurrence of Ultramicroscopic Bodies with Leafhoppers and Mosquitoes. *Bull. Brooklyn Entomol. Soc.* **1952**, *47*, 41−42.
(26) Kroto, H. W.; Heath, J. R.; O'Brien, S. C.; Curl, R. F.; Smalley, R. E. C 60: Buckminsterfullerene. *Nature* **1985**, *318*, 162−163.
(27) Tulloch, G. S.; Shapiro, J. E. Brochosomes. *Bull. Brooklyn Entomol. Soc.* **1953**, *48*, 57−63.
(28) Rakitov, R.; Moysa, A. A.; Kopylov, A. T.; Moshkovskii, S. A.; Peters, R. S.; Meusemann, K.; Misof, B.; Dietrich, C. H.; Johnson, K. P.; Podsiadlowski, L.; Walden, K. K. O. Brochosomins and Other Novel Proteins from Brochosomes of Leafhoppers (Insecta, Hemiptera, Cicadellidae). *Insect Biochem. Mol. Biol.* **2018**, *94*, 10−17.
(29) Rakitov, R. A. The Covering Formed by Brochosomes on the Cuticle of Leafhoppers (Homoptera, Cicadellidae). *Entomol.Rev.* **1995**, *74*, 90−103.
(30) Wilde, W. H. A.; Cochrane, G. W. Brochosomes on Certain Species of Insects of Western North America. *J. Entomol. Soc. B. C.* **1957**, *53*, 19−20.
(31) Li, W.; Liu, L.; Xu, L.; Zhang, J.; Yuan, Q.; Ding, X.; Hu, W.; Fu, P.; Zhang, D. Overview of Primary Biological Aerosol Particles from a Chinese Boreal Forest: Insight into Morphology, Size, and Mixing State at Microscopic Scale. *Sci. Total Environ.* **2020**, *719*, 137520.
(32) Wittmaack, K. Brochosomes Produced by Leafhoppers-a Widely Unknown, yet Highly Abundant Species of Bioaerosols in Ambient Air. *Atmos. Environ.* **2005**, *39*, 1173−1180.
(33) Wittmaack, K.; Wehnes, H.; Heinzmann, U.; Agerer, R. An Overview on Bioaerosols Viewed by Scanning Electron Microscopy. *Sci. Total Environ.* **2005**, *346*, 244−255.
(34) Rakitov, R.; Gorb, S. N. Brochosomal Coats Turn Leafhopper (Insecta, Hemiptera, Cicadellidae) Integument to Superhydrophobic State. *Proc. R. Soc. B* **2013**, *280*, 20122391.
(35) Rakitov, R.; Gorb, S. N. Brochosomes Protect Leafhoppers (Insecta, Hemiptera, Cicadellidae) from Sticky Exudates. *J. R. Soc., Interface* **2013**, *10*, 20130445.
(36) Shih, M.-S.; Chen, H.-Y.; Li, P.-C.; Yang, H. Broadband Omnidirectional Antireflection Coatings Inspired by Embroidered Ball-like Structures on Leafhoppers. *Appl. Surf. Sci.* **2020**, *532*, 147397.
(37) Hua, C.; Cheng, Z.; Ma, Y.; He, H.; Xu, G.; Liu, Y.; Yang, S.; Han, G. Enhanced Electrochromic Tungsten Oxide by Bio-Inspired Brochosomes. *J. Electrochem. Soc.* **2021**, *168*, 042503.
(38) Pan, Q.; Zhang, H.; Yang, Y.; Cheng, C. 3D Brochosomes-Like TiO2/WO3/BiVO4 Arrays as Photoanode for Photoelectrochemical Hydrogen Production. *Small* **2019**, *15*, 1900924.
(39) Rakitov, R. *What Are Brochosomes for? An Enigma of Leafhoppers (Hemiptera, Cicadellidae)*; Russian Academy of Sciences, 2002.

https://doi.org/10.1021/acs.biomac.2c01035
Biomacromolecules 2023, 24, 190−200

(40) Laramy, C. R.; Brown, K. A.; O'Brien, M. N.; Mirkin, C. A. High-Throughput, Algorithmic Determination of Nanoparticle Structure from Electron Microscopy Images. *ACS Nano* **2015**, *9*, 12488−12495.
(41) Kim, J.; Jones, M. R.; Ou, Z.; Chen, Q. In Situ Electron Microscopy Imaging and Quantitative Structural Modulation of Nanoparticle Superlattices. *ACS Nano* **2016**, *10*, 9801−9808.
(42) Kim, J.; Song, X.; Kim, A.; Luo, B.; Smith, J. W.; Ou, Z.; Wu, Z.; Chen, Q. Reconfigurable Polymer Shells on Shape-Anisotropic Gold Nanoparticle Cores. *Macromol. Rapid Commun.* **2018**, *39*, 1800101.
(43) Wang, X.; Li, J.; Ha, H. D.; Dahl, J. C.; Ondry, J. C.; Moreno-Hernandez, I.; Head-Gordon, T.; Alivisatos, A. P. AutoDetect-MNP: An Unsupervised Machine Learning Algorithm for Automated Analysis of Transmission Electron Microscope Images of Metal Nanoparticles. *JACS Au* **2021**, *1*, 316−327.
(44) Yao, L.; Ou, Z.; Luo, B.; Xu, C.; Chen, Q. Machine Learning to Reveal Nanoparticle Dynamics from Liquid-Phase Tem Videos. *ACS Cent. Sci.* **2020**, *6*, 1421−1430.
(45) Rizvi, A.; Mulvey, J. T.; Carpenter, B. P.; Talosig, R.; Patterson, J. P. A Close Look at Molecular Self-Assembly with the Transmission Electron Microscope. *Chem. Rev.* **2021**, *121*, 14232−14280.
(46) Patterson, J. P.; Sanchez, A. M.; Petzetakis, N.; Smart, T. P.; Epps, T. H., III; Portman, I.; Wilson, N. R.; O'Reilly, R. K. A Simple Approach to Characterizing Block Copolymer Assemblies: Graphene Oxide Supports for High Contrast Multi-Technique Imaging. *Soft Matter* **2012**, *8*, 3322−3328.
(47) Smith, A. M.; Williams, R. J.; Tang, C.; Coppo, P.; Collins, R. F.; Turner, M. L.; Saiani, A.; Ulijn, R. V. Fmoc-Diphenylalanine Self Assembles to a Hydrogel via a Novel Architecture Based on π-π Interlocked β-Sheets. *Adv. Mater.* **2008**, *20*, 37−41.
(48) Hong, F.; Zhang, F.; Liu, Y.; Yan, H. DNA Origami: Scaffolds for Creating Higher Order Structures. *Chem. Rev.* **2017**, *117*, 12584−12640.
(49) Kuzuya, A.; Komiyama, M. DNA Origami: Fold, Stick, and Beyond. *Nanoscale* **2010**, *2*, 309−321.
(50) Pinheiro, A. V.; Han, D.; Shih, W. M.; Yan, H. Challenges and Opportunities for Structural DNA Nanotechnology. *Nat. Nanotechnol.* **2011**, *6*, 763−772.
(51) Cai, W.; Li, C. Y.; Li, L.; Lotz, B.; Keating, M.; Marks, D. Submicrometer Scroll/Tubular Lamellar Crystals of Nylon 6, 6. *Adv. Mater.* **2004**, *16*, 600−605.
(52) Hanemann, T.; Szabó, D. V. Polymer-Nanoparticle Composites: From Synthesis to Modern Applications. *Materials* **2010**, *3*, 3468−3517.
(53) Besenius, P.; Portale, G.; Bomans, P. H.; Janssen, H. M.; Palmans, A. R.; Meijer, E. Controlling the Growth and Shape of Chiral Supramolecular Polymers in Water. *Proc. Natl. Acad. Sci. U.S.A.* **2010**, *107*, 17888−17893.
(54) Dmitriev, D. A. 31, a New Program for Creating Internet-Accessible Interactive Keys and Taxonomic Databases and Its Application for Taxonomy of Cicadina (Homoptera). *Russ. Entomol. J.* **2006**, *15*, 263−268.
(55) Hajibabaei, M.; Janzen, D. H.; Burns, J. M.; Hallwachs, W.; Hebert, P. D. DNA Barcodes Distinguish Species of Tropical Lepidoptera. *Proc. Natl. Acad. Sci. U.S.A.* **2006**, *103*, 968−971.
(56) Ratnasingham, S.; Hebert, P. D. A DNA-Based Registry for All Animal Species: The Barcode Index Number (BIN) System. *PLoS One* **2013**, *8*, No. e66213.
(57) Schindelin, J.; Arganda-Carreras, I.; Frise, E.; Kaynig, V.; Longair, M.; Pietzsch, T.; Preibisch, S.; Rueden, C.; Saalfeld, S.; Schmid, B.; Tinevez, J.-Y.; White, D. J.; Hartenstein, V.; Eliceiri, K.; Tomancak, P.; Cardona, A. Fiji: An Open-Source Platform for Biological-Image Analysis. *Nat. Methods* **2012**, *9*, 676−682.
(58) Kremer, J. R.; Mastronarde, D. N.; McIntosh, J. R. Computer Visualization of Three-Dimensional Image Data Using IMOD. *J. Struct. Biol.* **1996**, *116*, 71−76.
(59) Yan, R.; Venkatakrishnan, S. V.; Liu, J.; Bouman, C. A.; Jiang, W. MBIR: A Cryo-ET 3D Reconstruction Method That Effectively Minimizes Missing Wedge Artifacts and Restores Missing Information. *J. Struct. Biol.* **2019**, *206*, 183−192.
(60) Rakitov, R.; Appel, E. Life History of the Camelthorn Gall Leafhopper, *Scenergates Viridis* (Vilbaste) (Hemiptera, Cicadellidae). *Psyche J. Entomol.* **2012**, *2012*, 1−19.
(61) Jakšić, Z.; Obradov, M.; Jakšić, O. Brochosome-Inspired Metal-Containing Particles as Biomimetic Building Blocks for Nanoplasmonics: Conceptual Generalizations. *Biomimetics* **2021**, *6*, 69.
(62) Mill, L.; Wolff, D.; Gerrits, N.; Philipp, P.; Kling, L.; Vollnhals, F.; Ignatenko, A.; Jaremenko, C.; Huang, Y.; De Castro, O.; Audinot, J. N.; Nelissen, I.; Wirtz, T.; Maier, A.; Christiansen, S. Synthetic Image Rendering Solves Annotation Problem in Deep Learning Nanoparticle Segmentation. *Small Methods* **2021**, *5*, 2100223.
(63) Ziatdinov, M.; Dyck, O.; Maksov, A.; Li, X.; Sang, X.; Xiao, K.; Unocic, R. R.; Vasudevan, R.; Jesse, S.; Kalinin, S. V. Deep Learning of Atomically Resolved Scanning Transmission Electron Microscopy Images: Chemical Identification and Tracking Local Transformations. *ACS Nano* **2017**, *11*, 12742−12752.
(64) Radmacher, M.; Cleveland, J. P.; Fritz, M.; Hansma, H. G.; Hansma, P. K. Mapping Interaction Forces with the Atomic Force Microscope. *Biophys. J.* **1994**, *66*, 2159−2165.
(65) Garcia, R. Nanomechanical Mapping of Soft Materials with the Atomic Force Microscope: Methods, Theory and Applications. *Chem. Soc. Rev.* **2020**, *49*, 5850−5884.
(66) Dimitriadis, E. K.; Horkay, F.; Maresca, J.; Kachar, B.; Chadwick, R. S. Determination of Elastic Moduli of Thin Layers of Soft Material Using the Atomic Force Microscope. *Biophys. J.* **2002**, *82*, 2798−2810.
(67) Wenger, M. P.; Bozec, L.; Horton, M. A.; Mesquida, P. Mechanical Properties of Collagen Fibrils. *Biophys. J.* **2007**, *93*, 1255−1263.
(68) Sagvolden, G.; Giaever, I.; Feder, J. Characteristic Protein Adhesion Forces on Glass and Polystyrene Substrates by Atomic Force Microscopy. *Langmuir* **1998**, *14*, 5984−5987.
(69) Zhang, Y.; Zhu, X.; Chen, B. Adhesion Force Evolution of Protein on the Surfaces with Varied Hydration Extent: Quantitative Determination via Atomic Force Microscopy. *J. Colloid Interface Sci.* **2022**, *608*, 255−264.
(70) Rakitov, R. A. Powdering of Egg Nests with Brochosomes and Related Sexual Dimorphism in Leafhoppers (Hemiptera: Cicadellidae). *Zool. J. Linn. Soc.* **2004**, *140*, 353−381.

https://doi.org/10.1021/acs.biomac.2c01035
Biomacromolecules 2023, 24, 190−200